Submitted for publication in ApJL
Preprint typeset using LaTeX style emulateapj v. 12/16/11

THE PLACE OF THE LOCAL GROUP IN THE COSMIC WEB

J. E. Forero-Romero[1] and R. González[2]
[1] Departamento de Física, Universidad de los Andes, Cra. 1 No. 18A-10, Edificio Ip, Bogotá, Colombia
[2] Instituto de Astrofísica, Pontificia Universidad Católica, Av. Vicuña Mackenna 4860, Santiago, Chile

Submitted for publication in ApJL

ABSTRACT

In this Letter we explore the characteristics of the Local Group (LG) location in the cosmic web using a cosmological simulation in the ΛCDM cosmology. We use the Hessian of the gravitational potential to define the cosmic web, where regions are classified as either peak, sheet, filament or void. Results indicate: i) The LG pairs are preferentially located in filaments and sheets, ii) There is a strong signature that LG pairs orientation depends on the cosmic web, in particular for pairs in filaments/sheets the orbital angular momentum tends to be perpendicular to the filament direction or the sheet plane. iii) They are located in in a narrow range of local overdensity $0 < \delta < 4$, ellipticity $0.1 < e < 1.0$ and prolateness $-0.5 < p < 0.5$.

Subject headings: galaxies: Local Group — dark matter

1. INTRODUCTION

The configuration of galaxies in the Local Group (LG hereafter) is quite rare to find in the local Universe and in cosmological simulations. The LG is dominated by the two big spirals MW and M31, the next most-luminous galaxy is M33 which is $\sim$ 10 times less massive than M31, followed by several less luminous dwarf galaxies, up to a distance of $\sim$ 3Mpc. The velocity vector of M31, with a low tangential velocity is consistent to a head-on collision orbit toward the MW (Cox & Loeb 2008; van der Marel et al. 2012b; Sohn et al. 2012).

Another feature of the Local group is the relatively low velocity dispersion of nearby galaxies up to ~ 8 Mpc (Sandage & Tammann 1975; Aragon-Calvo et al. 2011, and references therein). Environment around the Local Group has density quite close to the average density of the universe (Klypin et al. 2003; Karachentsev 2005). In addition, the closest massive galaxy cluster, the Virgo Cluster, is ≈ 16.5 Mpc away (Mei et al. 2007).

All this combination of features make LG analogues very rare to find. Using numerical simulatons González et al. (2013a) found less than 2% MW-sized halos reside in a pair similar to MW-M31 and in a similar environment. Furthermore, if we select pairs constrained within 2σ error fron current observational measurements of the velocity components and distance to M31, there are only 46 systems in a cube of 250 h^{-1}Mpc side.

Forero-Romero et al. (2013) also studied MW-M31 pairs in numerical simulations finding the typical quantities characterizing the orbital parameters of the LG are rare among typical pairs, but not enough to challenge the ΛCDM model. Another definition of LG analogues is made by Li & White (2008), but despite differences ocurr in the definitions and resulting fraction of LG analogues, all are in agreement with a low frequency of these pairs.

To better understand the properties of the LG and how this uncommon pair configuration fit in the cosmological context, an immediate question arise. What else can we say of the LG at larger scales?. In particular, which are the typical/prefered locations of these systems within the Cosmic Web?.

Looking the LG at larger scales we have it is located in a difuse and warped filament/wall conecting Virgo Cluster with Fornax Cluster, some nearby galaxies and groups members of this large structure are the Maffei group, NGC 6744, NGC 5128, $M101$, $M81$, $NGC1023$, Cen A group. At this scale, there is no evident alignment of the MW-M31 orbital plane with the local filament or the Virgo-Fornax direction. However, if we look in a smaller volume below scales of ~ 6 Mpc, there is a clear alignment of th the MW-M31 orbit with a local plane as shown by figure 3 in Courtois et al. (2013).

The environment definition we use in this Letter uses the tidal tensor field.

In this Letter we study the large scale environment of LG analogues in the context of ΛCDM. We use the Bolshoi simulation to explore in what structures they reside and if there is any correlation or alignment with the cosmic web. The large scale Environment is defined by the cosmic web components identified by Forero-Romero et al. (2009), and we use the LG analogues computed by González et al. (2013a). We pay spetial attention to quantify the kind of environment that hosts LG pairs and their alignments with respect to the prefered directions defined by the T-web.

This Letter is organized as follows. In Section 2 we present the N-body cosmological simulation and the algorithm to define the cosmic web, next in 3 we describe the sample of LG analogues extracted from the simulation. In Section 4 we presents our results to continue with a discussion about their implications for our Local Group in Section 5 to finally conclude in Section 6.

2. SIMULATION AND WEB FINDING ALGORITHM

2.1. *The Bolshoi simulation*

We use the Bolshoi simulation of ΛCDM cosmology: $\Omega_{\rm m} = 1 - \Omega_\Lambda = 0.27$, $H_0 = 70\,{\rm km/s/Mpc}$, $\sigma_8 = 0.82$, $n_s = 0.95$ (Klypin et al. 2011), compatible with the constraints from the WMAP satellite (Hinshaw et al. 2013).

Electronic address: je.forero@uniandes.edu.co

The simulation followed evolution of dark matter in a $250h^{-1}$Mpc box with spatial resolution of $\approx 1h^{-1}$ kpc and mass resolution of $m_{\rm p} = 1.35 \times 10^8$ M$_\odot$. Halos are identified with the BDM algorithm (Klypin & Holtzman 1997). The BDM algorithm is a spherical overdensity halo finding algorithm and is designed to identify both host halos and subhalos.

2.2. *Cosmic web identification*

The web finding algorithm is based on the tidal tensor computed as the Hessian of the gravitational potential field

$$T_{ij} = \frac{\partial^2 \phi}{\partial r_i \partial r_j}, \quad (1)$$

where r_i, $i = 1, 2, 3$ refers to the three spatial comoving coordiates and ϕ is the gravitational potential renormalized to follow the following Poisson equation $\nabla^2 \phi = \delta$ where δ is the matter overdensity.

This tensor is real and symmetric, which means that can be diagonalized. We note its eigenvalues as $\lambda_1 \geq \lambda_2 \geq \lambda_3$ and their corresponding eigenvectors $\hat{e}_1$, $\hat{e}_2$ and $\hat{e}_3$. The web classification compares each one of the three eigenvalues to a threshold value $\lambda_{\rm th}$. If the three, two, one or zero eigenvalues are larger than this threshold the region is classified as peak, filament, sheet or void, respectively.

Forero-Romero et al. (2009) performed a detailed study for the topology of the cosmic web and its visual counterpart as a function of the parameter $\lambda_{\rm th}$. They found that reasonable results in terms of the volume fraction occupied by voids, the visual inspection and the halo populations in each web type can be reached by values of $0.2 < \lambda_{\rm th} < 0.4$. In this Letter we choose the value of $\lambda_{\rm th} = 0.3$ to proceed with our analysis. We have veryfied that the main trends reported in this paper are unsensitive to the choice of that parameter, as long as it is in the range already quoted.

The algorithm to compute the potential is grid based. First we interpolate the density into a cubic grid with a Cloud-In-Cell (CIC) scheme and smooth it with a gaussian kernel. Then we obtain the gravitational potential using FFT methods and use finite differences to compute the Hessian at every point in the grid. In our case we have used a grid size on and a gaussian smoothing with two times larger as the typical separation between the two halos in the Local Group. The purpose of this choice is to have both halos in the pair a common environment. In this paper we use a grid spacing of $s = 0.97$ h^{-1}Mpc , corresponding to a 256^3 grid in the Bolshoi volume. The scale for the gaussian smoothing uses the same value.

After computing the eigenvalues and eigenvectors on each point of the grid we use the matter overdensity, ellipticity and the prolatenes to further characterize the web. These quantities are defined in terms of the eigenvalues as follows

$$\delta = \lambda_1 + \lambda_2 + \lambda_3, \quad (2)$$

$$e = \frac{\lambda_3 - \lambda_1}{2(\lambda_1 + \lambda_2 + \lambda_3)}, \quad (3)$$

$$p = \frac{\lambda_1 + \lambda_3 - 2\lambda_2}{2(\lambda_1 + \lambda_2 + \lambda_3)}. \quad (4)$$

We are also interested in measuring the alignment of the LG halos with respect to the cosmic web. To this end we characterize each LG pair by the vector that is normal to the orbital plane, which is defined by the position and velocities of each halo with respect to the center of mass.

3. LOCAL GROUP ANALOGUES

To construct a sample of the MW-M31 pairs at $z \approx 0$, we use a series of simulation snapshots at $z < 0.1$ (since the last ≈ 1.3 Gyr) spaced by $\approx 150 - 250$ Myr. This is done because a particular configuration of MW and M31 is transient and corresponds to a relatively small number of systems at one snapshot. By using multiple snapshots we can increase the sample of systems in such configuration during a period of time in which secular cosmological evolution is small.

The LG analogues or General sample in this paper are pairs selected in relative isolation, and in a wide range of masses from $M_{200c} = 5 \times 10^{10}$ M$_\odot$ to 5×10^{13} M$_\odot$. Isolation criteria includes a pair closer than 1.3Mpc, and with no massive neighbors within 5Mpc. In addition we require that pairs have no Virgo-like neighbor halo with mass $M_{200c} > 1.5 \times 10^{14}$ M$_\odot$ within 12 Mpc. We have 5480 pairs under these general criteria. A full description of the selection criteria can be found in González et al. (2013a,b).

We also define two subsamples more closely related to the MW-M31 dynamics according to the tolerance in additional constraints: A sample named 2σ, correspondig to LG analogues constrained by two times the observational errors in the orbital values (radial velocity, tangential velocity, and separation), and a more relaxed sample named 3σ for LG analogues constrained by three times observational errors accordingly. The number of pairs in each sample is 46 and 120 respectively, notice we have less pairs than in González et al. (2013a) results, since we removed pairs which are too close at $z = 0$, i.e. their virial radii overlaps, also we removed a couple pairs that merged or change their mass more than 20% at present time since they were detected at $z < 0.1$.

4. RESULTS

4.1. *The prefered environment for LGs*

The first result we explore is the kind of environment occupied by our LGs. We find that the LGs in the general sample are located across all different evironment without any strong preferences; 1/3 are located in sheets, 1/4 in peaks, 1/4 in filaments and the remaning 1/6 in voids.

The situation in the restricted 2σ and 3σ samples is very different. By large the LGs in these samples are located in filaments and sheets. In both samples, $\sim 50\%$ of the pairs can be found in filaments while $\sim 40\%$ are in in sheets. These absolute numbers in each environment for each sample are presented in Table 1.

This difference between the general and the restricted samples is mostly due the mass ranges covered by each sample. In González et al. (2013a) the mass range covered by 2σ and 3σ is very narrow and it is used to constraint the LG mass, then we show also in table 1 a subsample of the General sample having a similar mass range to 2σ and 3σ, and it reproduces similar environment fractions.

A more clear view of this environment dependency and pair mass is shown in figure 1, where we show the mass

Sample	Peak n (%)	Filament n (%)	Sheet n (%)	Void n (%)
2σ	4 (8.7)	24 (52.2)	17 (36.7)	1 (2.2)
3σ	10 (8.3)	58 (48.3)	47 (39.2)	5 (4.2)
General ($12.1 < \log_{10} M_{\rm h}/{\rm M}_\odot < 12.3$)	8 (1.4)	334 (55.5)	259 (43.0)	1 (0.1)
General	1312 (23.9)	1472 (26.9)	1769 (32.3)	927 (16.9)

TABLE 1
NUMBER OF PAIRS IN THE FOUR DIFFERENT KINDS OF ENVIRONMENTS. IN PARETHESIS THE SAME NUMBER AS A PERCENTAGE OF THE TOTAL POPULATION.

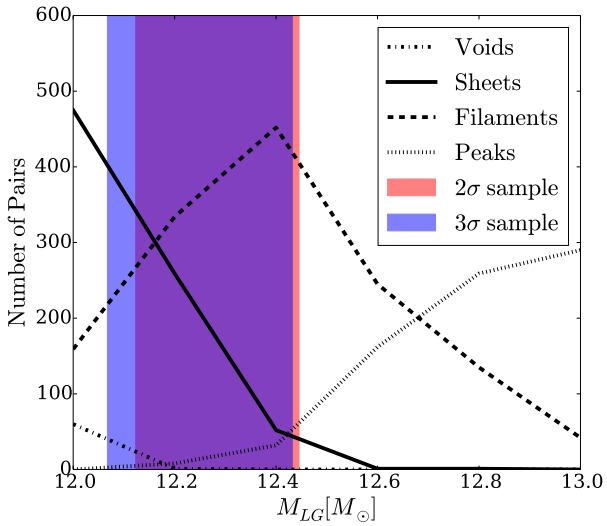

FIG. 1.— Mass distribution of pairs in the different environments for the General sample. Dashed regions correspond to the mass ranges of 2σ and 3σ samples.

distribution of pairs in the different environments, then high mass pairs tend to be located in peaks and filaments, and less massive ones in voids and sheets. Dashed regions represent the 68% confidence intervals of the mass distributions of 2σ and 3σ samples.

4.2. *Alignment along the cosmic web*

We explore the alignment of the pairs with respect to the cosmic web. We define the unit vector $\hat{n}$, normal to the pair orbital plane computed from the pair positions and relative velocity. Then, we compute the dot product of $\hat{n}$ and each one of the three eigenvectors for the three samples.

In Figure 2 we show the main result of that study, it presents the cumulative distribution of $\mu \equiv \hat{e}_i \cdot \hat{n}$ for the three eigenvectors $i = 1, 2, 3$. Lines indicate the different samples. The straight line corresponds to the expected result for a random vector distribution.

From this Figure we can see two important features: First, there is a strong anti-alignment signature between $\hat{n}$ and the third eigenvector, and this signature reverses with the first eigenvector. However, in the case of the second eigenvector, no significant deviations are found. Second, for $\hat{e}_3$ vector the anti-alignment become stronger for the samples more closely related to the LG, then for 2σ it is stronger than for 3σ, and the latter is stronger than for General sample.

Quantitatively, the anti-alignment feature found with

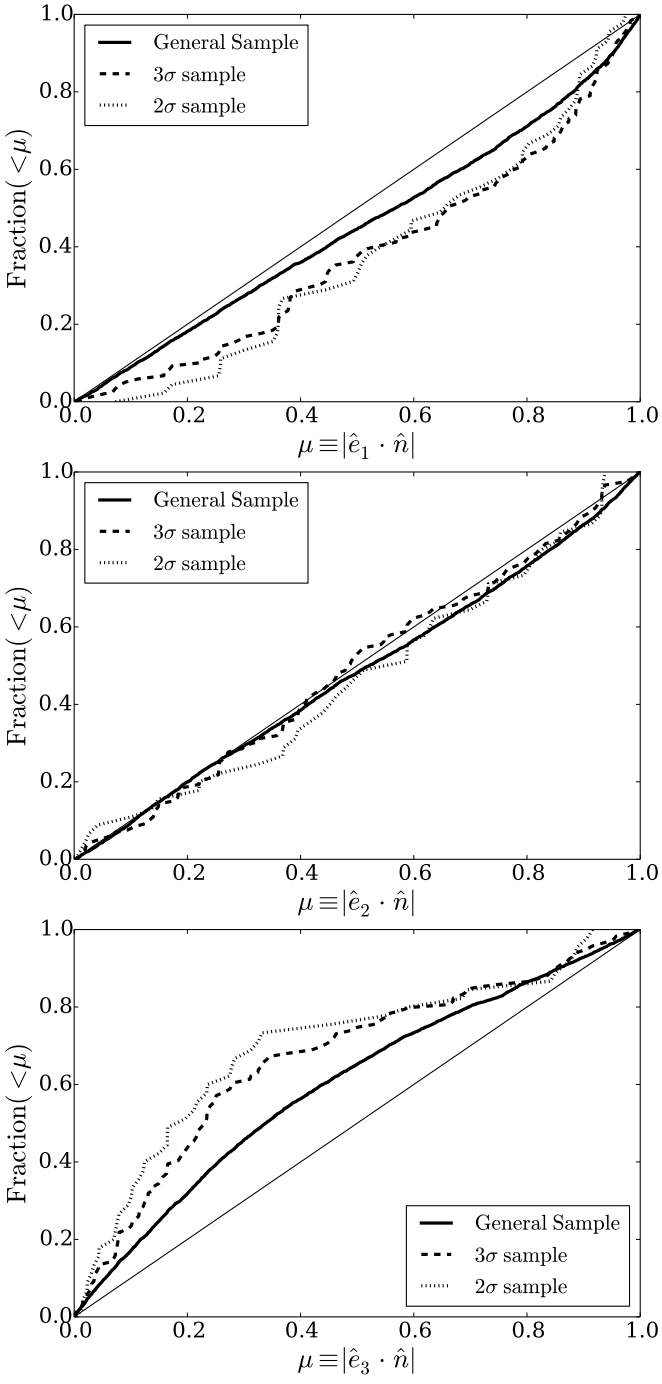

FIG. 2.— Cumulative distributions for the alignment between the normal vector to the pair orbit $\hat{n}$, and the eigenvectors defining the cosmic web.

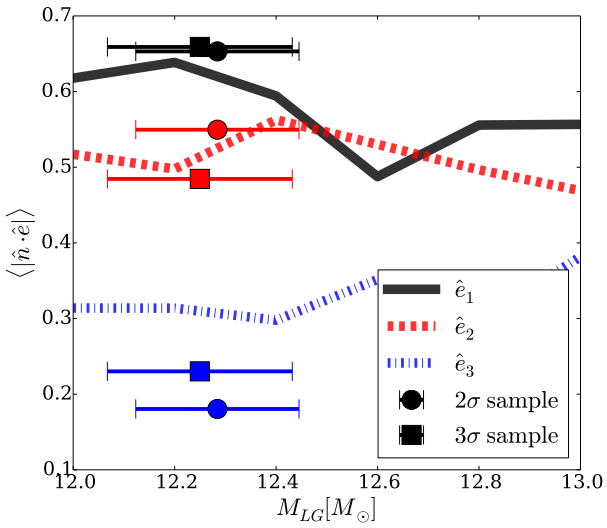

FIG. 3.— Mass dependency of the median value for the dot product between the normal vector $\hat{n}$ and each one of the eigenvectors. The lines show the trends for the general sample.

the $\hat{e}_3$ vector means that for 2σ sample, $\sim 50\%$ pairs have $\mu < 0.2$, and $\sim 75\%$ pairs have $\mu < 0.4$. We also test that does not change significantly on environment type, in particular these trends hold very well for pairs in filaments and walls.

If we consider only pairs in filaments, we have that the pair orbit tends to be perpendicular to the filament direction, and both pair members lie along the filament, if we recall the 3σ-2σ samples are constrained with a mostly radial velocity component, then the pairs are moving into the filament. In the case of sheets, we have the pair orbital plane tend to lie within the sheet plane.

These alignment features are in agreement with the scenario that pairs created in-situ or falling into a filament/wall align their orbits with the large scale structure in a relaxation process where pair members tend to moves along the slowest collapsing directions. However, the most intriguing feature is the dependence of this alignment with how close we represent the LG, is still not clear. We explore if the pair masses are responsible of this, but we found no dependence at all.

In Figure 3 we show the relation between the median of $\mu \equiv \hat{e}_i \cdot \hat{n}$ and mass for the general sample, and found no significant relation. Lines in the figure show the median μ-mass relation for the three eigenvectors in the General sample. Dots represent the median μ for the three eigenvectors in the 2σ-3σ samples. In the case of $\|\hat{e}_3 \cdot \hat{n}\|$, the figure clearly shows for a fixed mass range around $1.5 - 2.0 \times 10^{10}$ $M_\odot$, that the median μ decreases as we better constraint the LG samples, being larger for General sample and smaller for 2σ sample accordingly.

4.3. *Overdensity, Ellipticity and Anisotropy*

We now describe the preferred place of the LG samples in terms of the overdensity, ellipticiy and anisotropy as defined in Section 2.

Figure 4 shows dependency of overdensity, ellipciticy, and prolateness on pair mass for the different samples. General sample is represented by the solid lines with the associated errors covered by the shaded region.

Left panel shows the overdensity dependence on mass where higher mass pairs are located in high density regions. The 2σ and 3σ samples having a narrower mass range as shown in previous figure, are consequently located within a narrower range of overdensities $0.0 < \delta < 4.0$ peaking at $\delta \sim 1$. This is also consistent with the fact that these samples are mostly found in filaments and sheets. Average overdensity of 2σ and 3σ samples show no significant difference from the General sample within the same mass range.

Middle and right panels show web ellipciticy and absolute prolateness dependence on mass. Again we noticed that within the same mass range, the 2σ and 3σ average ellipciticy and prolateness does not differ significantly from General sample. For the 2σ and 3σ samples most of the pairs are located in a narrow range for ellipticities in the range $0.1 < e < 1.0$, and prolateness $0.5 < p < 0.5$.

4.4. *Spin and Orbital Angular Momentum*

In 4.2 we defined the unit vector $\hat{n}$, normal to the pair orbital plane which can be asociated with the orbital angular momentum direction $\hat{J}$. There, we show several alignment features of the pair orbital momentum with the environment. In this subsection we explore the alignement of the individual spin angular momentum of each pair member $\hat{j_A}$ and $\hat{j_B}$ with each other and with the orbital angular momentum.

We show in figure 5 the cumulative distribution of dot product between the spin of both members in the pair. We found a slight alignment of spin vectors for the 2σ sample. However, we found no significant alignment between spin and orbital angular momentum for any sample.

In the LG, the angle between MW and M31 spin is $\sim 60°$ and the angles between spins and orbital angular momentum are $\sim 33°$ and $\sim 76°$ for MW and M31 respectively (van der Marel et al. 2012a). Then the LG show no particular alignement aswell.

5. DISCUSSION

We explored the characteristics of the LG location in the cosmic web.

LG pairs are preferentially located in filaments and sheets. The mass range of the pairs sample plays an important role in the fractions for each environment type as shown in table 1 and figure 1.

There is a clear anti-alignment between the third eigenvector and the vector normal to the pair orbital plane. This feature is not mass dependant as can be shown in figure 3. For pairs in filaments this means the pair orbit tends to be perpendicular to the filament direction, and both pair members lie along the filament, and in the case of pairs in sheets, we have the pair orbital plane lie in the sheet plane. We also found this anti-alignment becomes stronger for the samples being more closely related to the LG, it means it is stronger for 2σ sample. All these alignment features are consistent with pair orbits relaxing their movements towards the slowest collapsing directions at larger scales.

LG pairs are located in a narrow range of local overdensity, ellipciticy and prolateness. And this is consistent with the narrow mass range selection of specific samples.

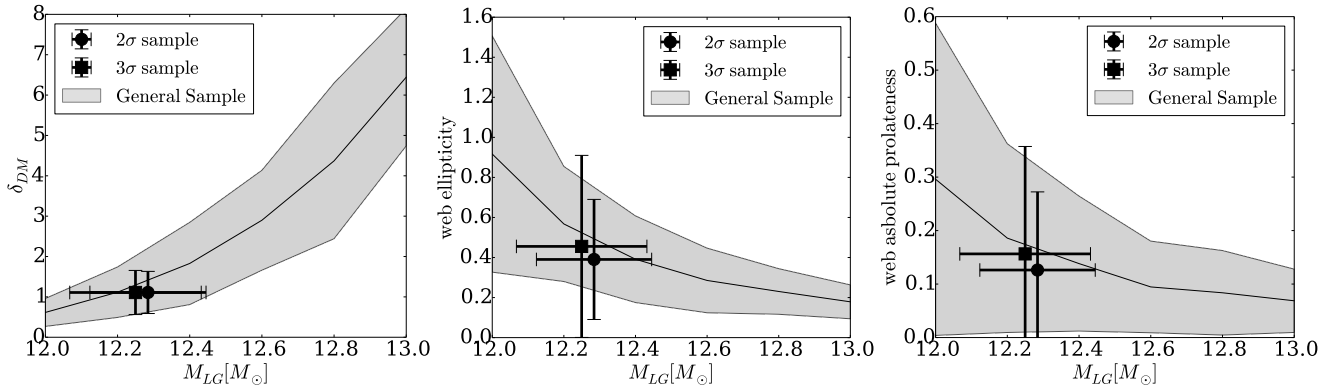

FIG. 4.— Mass dependency of the average dark matter overdensity (left), web ellipticity (middle) and web absolute value prolateness (right) at the pair location.

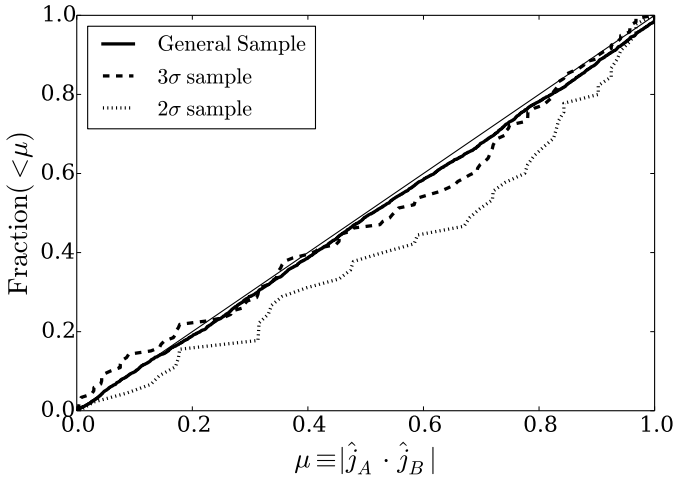

FIG. 5.— Alignment between the two angular momentum vectors of the two halos in the pair.

The LG spin and orbital angular momentum have no particular alignment, and we see no significan alignments in our LG pairs, however for the alignment between pair spins we found a slight alignment signature for 2σ sample as can be seen in figure 5.

6. CONCLUSIONS

ACKNOWLEDGEMENTS

REG was supported by Proyecto Financiamiento Basal PFB06 and Comite Mixto ESO.

REFERENCES

Aragon-Calvo, M. A., Silk, J., & Szalay, A. S. 2011, MNRAS, 415, L16
Courtois, H. M., Pomarède, D., Tully, R. B., Hoffman, Y., & Courtois, D. 2013, AJ, 146, 69
Cox, T. J., & Loeb, A. 2008, MNRAS, 386, 461
Forero-Romero, J. E., Hoffman, Y., Bustamante, S., Gottlöber, S., & Yepes, G. 2013, ApJ, 767, L5
Forero-Romero, J. E., Hoffman, Y., Gottlöber, S., Klypin, A., & Yepes, G. 2009, MNRAS, 396, 1815
González, R. E., Kravtsov, A. V., & Gnedin, N. Y. 2013a, ArXiv e-prints
—. 2013b, ApJ, 770, 96
Hinshaw, G., Larson, D., Komatsu, E., Spergel, D. N., Bennett, C. L., Dunkley, J., Nolta, M. R., Halpern, M., Hill, R. S., Odegard, N., Page, L., Smith, K. M., Weiland, J. L., Gold, B., Jarosik, N., Kogut, A., Limon, M., Meyer, S. S., Tucker, G. S., Wollack, E., & Wright, E. L. 2013, ApJS, 208, 19
Karachentsev, I. D. 2005, AJ, 129, 178
Klypin, A., Hoffman, Y., Kravtsov, A. V., & Gottlöber, S. 2003, ApJ, 596, 19
Klypin, A., & Holtzman, J. 1997, ArXiv Astrophysics e-prints
Klypin, A. A., Trujillo-Gomez, S., & Primack, J. 2011, ApJ, 740, 102
Li, Y.-S., & White, S. D. M. 2008, MNRAS, 384, 1459
Mei, S., Blakeslee, J. P., Côté, P., Tonry, J. L., West, M. J., Ferrarese, L., Jordán, A., Peng, E. W., Anthony, A., & Merritt, D. 2007, ApJ, 655, 144
Sandage, A., & Tammann, G. A. 1975, ApJ, 196, 313
Sohn, S. T., Anderson, J., & van der Marel, R. P. 2012, ApJ, 753, 7
van der Marel, R. P., Besla, G., Cox, T. J., Sohn, S. T., & Anderson, J. 2012a, ApJ, 753, 9
van der Marel, R. P., Fardal, M., Besla, G., Beaton, R. L., Sohn, S. T., Anderson, J., Brown, T., & Guhathakurta, P. 2012b, ApJ, 753, 8